Title
Tethered peptide toxins for ion channels

ISBN
9780128239247

Authors
Zhao, Ruiming
Goldstein, Steve AN

Publication Date
2021

DOI
10.1016/bs.mie.2021.03.002

Tethered peptide toxins for ion channels

Ruiming Zhao and Steve A.N. Goldstein*
Departments of Pediatrics, Physiology & Biophysics, and Pharmaceutical Sciences, Susan and Henry Samueli College of Health Sciences, University of California, Irvine, CA, United States
*Corresponding author: e-mail address: sgoldst2@uci.edu

Contents

Abstract

In this method paper, we describe protocols for using membrane-tethered peptide toxins (T-toxins) to study the structure/function and biophysics of toxin-channel interactions with two-electrode voltage clamp (TEVC). Here, we show how T-toxins can be used to determine toxin equilibrium affinity, to quantify toxin surface level by enzyme-linked immunosorbent assay (ELISA) and/or single-molecule total internal reflection fluorescence (smTIRF) microscopy, to assess toxin association and dissociations rate, to identify toxin residues critical to binding via scanning mutagenesis, and to study of toxin blocking mechanism. The sea anemone type I (SAK1) toxin HmK and a potassium channel are used to demonstrate the strategies. T-toxins offer experimental flexibility that facilitates studies of toxin variants by mutation of the expression

Methods in Enzymology
ISSN 0076-6879
https://doi.org/10.1016/bs.mie.2021.03.002

plasmid, avoiding the need to synthesize and purify individual peptides, speeding and reducing the cost of studies. T-toxins can be applied to peptide toxins that target pores or regulatory domains, that inhibit or activate, that are derived from different species, and that bind to different types of ion channels.

1. Introduction

Venom peptide toxins from sea anemone, scorpion, spider, snake and cone snail that act on ion channels either physically occlude the conduction pore or modify channel gating (Kalia et al., 2015). Peptide toxins are powerful tools for studying the structure and function of ion channels (Bosmans, Martin-Eauclaire, & Swartz, 2008; Cordeiro et al., 2019; Goldstein, Pheasant, & Miller, 1994; Jiang et al., 2021; MacKinnon & Miller, 1989), and are used in medical diagnosis and therapy (Wulff, Christophersen, Colussi, Chandy, & Yarov-Yarovoy, 2019). The inspiration for tethered peptide toxins (T-toxin) was lynx1, an endogenous modulator of nicotinic acetylcholine receptors (nAChR) that is homologous to snake α-neurotoxins and naturally-tethered at the cell surface of mouse neurons via a glycosylphosphatidylinositol (GPI) anchor (Miwa et al., 1999). Subsequent to the description of lynx1, peptide toxins from a spider and a cone snail were purposefully tethered by encoding the toxin gene in-frame with the GPI signal and processing sequences of lynx1 and shown to express and modulate the function of voltage-gated sodium channels and calcium channels, respectively (Ibanez-Tallon et al., 2002, 2004). T-toxins expression constructs allow the encoded peptide toxins to pass through the protein secretory pathway, after which the N-terminal signal peptide sequence is cleaved by endogenous proteases, so the unadorned peptide is exposed on the surface, and the lynx1 GPI targeting sequence is removed so the toxin is linked covalently to GPI, anchoring the peptide to the extracellular leaflet of the plasma membrane in stable fashion. T-toxins appear to diffuse without limitation (on both poles of *Xenopus* oocytes) so they can interact with the external portions of surface ion channels, providing a new way to the regulate function *in vitro* and *in vivo* (Ibanez-Tallon & Nitabach, 2012). To-date, venom peptides from spiders, scorpions, snakes and sea anemone have been crafted as T-toxins and tested for potency on various membrane receptors (Gui et al., 2014; Ibanez-Tallon & Nitabach, 2012; Rupasinghe et al., 2020; Zhao, Dai, Mendelman, Chill, & Goldstein, 2020).

T-toxins have several useful attributes compared to their free peptide analogs. First, T-toxins can speed and reduce the costs of studies of toxin variants allowing their production by simple mutation of the expression construct; this is especially useful in scanning and, thereafter, in the iterative study of positions where examining successive hypothesis otherwise requires synthesis and purification of peptides, decreasing the time to study scores of variants from many months to just weeks. Second, T-toxins can be expressed at high levels close to their targets, concentrations that cannot be achieved for free peptides in solution, and thereby permit study of toxins with low affinities or to efficiently silent the target channels. Third, T-toxins can be selectively delivered to specific cell populations by viral vectors. Fourth, T-toxins tolerate engineering to incorporate additional useful modules, such as fluorescent proteins (Auer et al., 2010).

Thus, T-toxins have been successfully employed to silence neurotransmission (Auer et al., 2010), to dissect mammalian circuits *in vivo* (Choi et al., 2009), and to identify a natural peptide inhibitor of TRPA1 channels and study its residues by mutagenesis (Gui et al., 2014). Recently, we extended the use of T-toxins to scanning mutagenesis of two native sea anemone toxins (HmK and ShK) and one designer toxin (Hui1) that block the ion conduction pores in two K^+ channels (KcsA and Kv1.3) to characterize the biophysical parameters of toxin blockade, including characterization of binding affinity and kinetic parameters of inhibition and to identify and vary residues important for binding, showing the approach can be used to help define modes and mechanisms of toxin action (Zhao et al., 2020).

For these reasons, we now employ T-toxins to scan peptide toxins and then confirm inferred mechanisms with a few soluble peptides. The most apparent limitations of the approach include the need to validate that the parent toxin acts similarly in soluble and tethered form, that surface expression of variants does not verify correct folding (although the same challenge exists for soluble congeners, HPLC purification and MS almost always provide forewarning), and an anticipated problem we have yet to observe that since the toxin C-terminus is tethered binding that requires its free exposure for interaction will be precluded.

In Sections 2–5, we describe methods for (1) determining T-toxin equilibrium affinity via quantification of current inhibition by two-electrode voltage clamp (TEVC) and estimation of local T-toxin concentration by enzyme-linked immunosorbent assay (ELISA) and single-molecule total internal reflection fluorescence (smTIRF) microscopy; (2) determining T-toxin association rate after rapid release from tetraethylammonium (TEA) blockade,

and calculation of the T-toxin dissociation rate from the measured association rate and equilibrium affinity; (3) identification of T-toxin residues critical to binding via scanning mutagenesis; and (4) study of T-toxin blocking mechanism. We demonstrate the methods with HmK, a sea anemone type I (SAK1) toxin, and the pore of KcsA carried in a Shaker channel (KcsA-Shaker).

2. Measuring T-HmK equilibrium affinity for KcsA-shaker channels in *Xenopus* oocytes (Figs. 1 and 2)

Sea anemone type I (SAK1) toxins can be potent K^+ channel blockers (Diochot & Lazdunski, 2009). They are short peptides (35–37 residues) with a backbone scaffold stabilized by three disulfide bonds that were first isolated

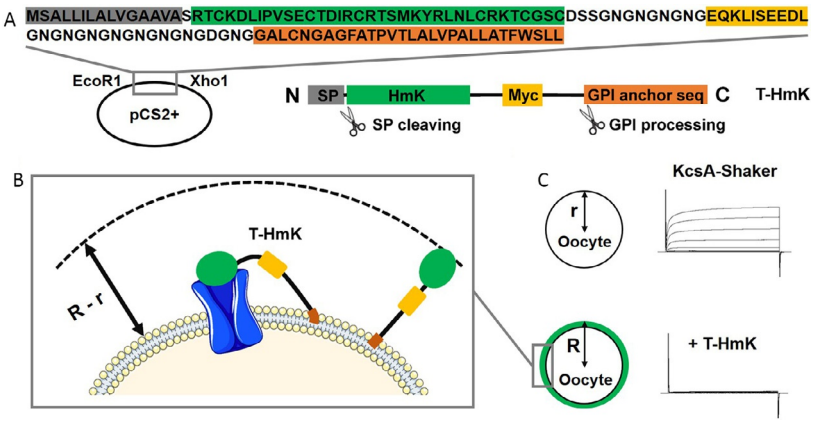

Fig. 1 Tethered HmK (T-HmK) blockade of KcsA-Shaker channels. (A) T-HmK was constructed as chimeric fusion protein with a N-terminal secretory signal sequence (SP, gray), the HmK toxin sequence (green), a hydrophilic flexible linker containing a c-Myc epitope tag (yellow), and a C-terminal GPI membrane anchor targeting sequence (orange). The T-HmK sequence was cloned into a pCS2+ plasmid vector using the restriction sites EcoR1 and Xho1 for synthesis of cRNA and expression in *Xenopus laevis* oocytes. (B) T-HmK binds to KcsA-Shaker (blue) co-expressed in the same oocyte. The reaction volume that a T-HmK can visit is determined by the cumulative length of the GPI anchor, the flexible peptide linker, and the diameter of HmK toxin (R − r). (C) KcsA-Shaker alone or +T-HmK was expressed on oocytes and studied by TEVC to assess inhibition at equilibrium from a holding voltage of −80 mV with 300-ms steps from −80 to 60 mV and 5 s interpulse intervals. Co-injection of 0.5 ng cRNA of T-HmK inhibited ~94% of the K+ current at 0 mV.

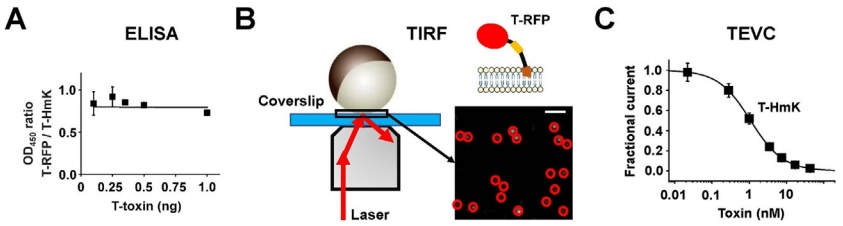

Fig. 2 T-HmK affinity determined by ELISA, smTIRF and TEVC. Oocytes were studied by ELISA, smTIRF microscopy and TEVC. (A) Oocytes were injected with increasing amounts of T-HmK or T-RFP cRNA. After 2 days culture, surface expression of T-HmK and T-RFP was determined by ELISA using anti-Myc-HRP. The ELISA signals for T-RFP and T-HmK show a stable relationship as the amount of injected cRNA increases. Two separate trials with six oocytes and five concentrations of T-HmK or T-RFP cRNA were measured. (B) 2 days after T-RFP cRNA injection, devitellinized oocytes were studied using smTIRF with 561 nm laser illumination. A single frame from a representative movie showing T-RFP on an oocyte membrane surface after 0.5 ng cRNA injection is shown. Red circles mark single fluorescent spots. White bar indicates 2 μm. (C) Concentration-response relationship for T-HmK inhibition of KcsA-Shaker studied by TEVC and fit to the Hill relationship (Eq. 1). The determined K_i was 1.09 ± 0.01 nM with a Hill coefficient of 1.00 ± 0.01. $n = 16$–18 oocytes for each level of injected T-HmK cRNA.

from Sea anemone stinging organelle cnidocytes (Diochot & Lazdunski, 2009). The SAK1 peptides ShK (Castaneda et al., 1995), HmK (Gendeh et al., 1997), and BgK (Cotton et al., 1997), block voltage-gated K^+ channels by occluding the ion conduction pore from the external side (Lanigan et al., 2002; Tudor, Pallaghy, Pennington, & Norton, 1996).

KcsA is a pH-activated prokaryotic K^+ channel from *Streptomyces lividans* formed by four identical subunits each with two transmembrane segments that assemble to form a single, central K^+ selective pore (Doyle et al., 1998). Seeking to redress the absence of identified high-affinity and specific inhibitors of the channel we screened a combinatorial, phage-display library of 1.5 million novel SAK1-related peptides on KcsA (Zhao et al., 2015). We identified two KcsA pore blockers, a natural SAK1 toxin (HmK with 35 residues), and a *de novo* toxin (Hui1) comprised of sequences derived from HmK and AETX-K (Zhao et al., 2015). HmK is promiscuous, blocking KcsA, Kv1.2, Kv1.3, and Shaker channels with half-maximal equilibrium inhibition constants (K_i) of 1–4 nM (whereas Hui1 is specific for KcsA, blocking the other channels 200-fold less well) (Zhao et al., 2015). Later, we studied T-HmK, T-ShK and their peptide analogs with KcsA-Shaker and hKv1.3, a human voltage-gated K^+ channel that is essential for T lymphocyte function (Chandy & Norton, 2017; Takacs et al., 2009),

observing that HmK peptide and T-HmK and point mutant variants block with a similar affinity and by the same mechanism, inserting a conserved Lys_{22} into the channel ion conduction pores (Zhao et al., 2020). Conversely, we found that T-ShK and ShK unexpectedly block hKv1.3 via a conserved Arg_{24} near the pore rather than via a canonical lysine in the selectivity filter like HmK and other pore-directed K^+ channel blockers (Goldstein & Miller, 1993; MacKinnon & Miller, 1988). Here, we outline how to study the biophysics of toxin-channel interaction with T-toxins by describing the use of T-HmK.

To demonstrate the T-toxin method, we employ free HmK, a natural peptide in the sea anemone *Heteractis magnifica* (Gendeh et al., 1997) that blocks KcsA-Shaker (and KcsA) as a free peptide with a K_i of 1 nM (Zhao et al., 2015) and the T-HmK expression plasmid that also blocks with a K_i of 1 nM (Zhao et al., 2020). The transplantation of the KcsA pore into a Shaker voltage-gated K^+ channel (KcsA-Shaker) is also described (Lu, Klem, & Ramu, 2001; Zhao et al., 2015). cRNAs for T-HmK and KcsA-Shaker are synthesized *in vitro* and co-injected into *Xenopus* oocytes.

2.1 Materials

1. The T-HmK plasmid was constructed by cloning the sequence of HmK (RTCKDLIPVSECTDIRCRTSMKYRLNLCRKTCGSC, GenBank# U58107.1) into a pCS2+ plasmid vector (https://www.addgene.org/vector-database/2295/) between a trypsin secretory signal peptide sequence and a flexible 46-residue linker with an embedded c-Myc epitope that was followed by a GPI targeting sequence using PCR (Fig. 1A). pCS2+ has a SP6 promoter for *in vitro* transcription.
2. KcsA-Shaker was constructed using gBlocks Gene Fragments (Integrated DNA Technologies) and inserted into pMAX+ vector using Gibson Assembly (New England BioLabs). Each KcsA-Shaker subunit carries the four transmembrane spans that form the Shaker channel voltage-sensing domain (S1–S4) with the native S5–S6 pore-forming segments replaced by KcsA residues (Lu et al., 2001). pMAX+ is a Goldstein laboratory vector available on request with the 5′ and 3′ portions of the *Xenopus laevis* β-globin gene, and a T7 promoter for transcription.
3. cRNAs for T-HmK and KcsA-Shaker were synthesized *in vitro*. The plasmids were linearized using *Not*I-HF (New England BioLabs), purified using QIAquick PCR Purification Kit (QIAGEN), and cRNAs synthesized using the mMESSAGE mMACHINE kit for SP6 or T7 (Invitrogen), respectively. cRNAs were diluted with RNase-free

water, concentrations were measured using NanoDrop 2000 (Thermo Fisher Scientific) and stored at −80 °C until use.

4. *Xenopus* oocytes were purchased from commercial sources (Xenoocyte, Ecocyte or Nasco). Oocytes with stage VI morphology were selected based on visual inspection of size and clear white equatorial bands. Detailed information about *Xenopus* oocytes selection and handling has been described (Stuhmer, 1998). Oocytes before and after injection were maintained in (Standard Oocyte Solution) SOS solution at 16 °C.
5. The SOS solution contains in mM: 2 KCl, 100 NaCl, 1.8 $CaCl_2$, 1 $MgCl_2$, 10 HEPES, 0.1 EDTA, 2 Na-pyruvate, pH 7.4, with 100 IU/mL penicillin and 100 μg/mL streptomycin. The Na-pyruvate allows oocytes to remain viable for longer periods.
6. The OR2 (Oocyte Ringer's Solution) solution contains in mM: 2.5 KCl, 82.5 NaCl, 1 $MgCl_2$, 5 HEPES, pH 7.4, and is the solution used for oocyte injection. OR2 is nominally calcium-free to avoid activating the oocytes during cRNA injection.
7. Recording solution for two-electrode voltage clamp (TEVC) contains in mM: 4 KCl, 100 NaCl, 0.3 $CaCl_2$, 1 $MgCl_2$, 10 HEPES, pH 7.5.
8. T-RFP was constructed by replacing the sequence of HmK in the T-HmK plasmid with the gene for a monomeric red fluorescent protein (TagRFP-T, GenBank# EU582019.1) using PCR. The cRNA of T-RFP was made as described above for T-HmK.
9. Nunc 96-Well microplates (Thermo Fisher Scientific).
10. Bovine serum albumin (BSA, Fraction V, Thermo Fisher Scientific).
11. c-Myc Monoclonal Antibody (9E10)-HRP (horseradish peroxidase) (Invitrogen).
12. 1-Step Ultra TMB-ELISA Substrate Solution (Thermo Fisher Scientific).
13. Sulfuric acid (Sigma-Aldrich).

2.2 Equipment

1. Oocyte clamp amplifier OC-725C (Warner Instruments) and
2. Digidata 1322A digitizer (Axon Instruments).
3. Nanoject III Nanoliter Injector (Drummond).
4. PP-83 Pipette Puller (Narishige).
5. Homemade gravity driven perfusion system and oocyte chamber that allows constant flow of recording solution at 2 mL/min yielding chamber exchange in 5 s.

6. Epoch microplate spectrophotometer (BioTec).
7. Multicolor cellTIRF system (Olympus).

2.3 Protocol

1. Injection of *Xenopus* Oocytes with T-HmK and KcsA-Shaker cRNAs. Glass micropipettes (3-000-203-G/X, Drummond) for injection were pulled using PP-83 Pipette Puller and the tips cut to ~20 μm diameter. Micropipettes were backfilled with mineral oil using a MicroFil Flexible Needle (World Precision Instruments) and 1 mL syringe. T-HmK and KcsA-Shaker cRNAs were diluted and mixed at a 1:2 (w/w) ratio for co-injection. Two microliter of cRNA was drawn into the micropipette from a clean piece of Parafilm and used for injecting oocytes (via the vegetal hemisphere) in a Petri dish with OR2 solution. We typically inject a total volume of ~25 nL containing cRNA into each oocyte. In control groups, oocytes were injected with 1 ng KcsA-Shaker cRNA. In T-toxin groups, 0.5 ng T-HmK cRNA and 1 ng KcsA-Shaker cRNA were co-injected. Oocytes were moved back to SOS solution and maintained at 16 °C for 2 days.
2. Assessing inhibition by T-HmK of KcsA-Shaker channels by TEVC recording by comparing two groups of cells. Borosilicate micropipettes (G100TF-3, Warner Instruments) for TEVC were pulled using PP-83 Pipette Puller and filled with 3 M KCl to give a electrodes resistance of 0.3–0.5 MΩ in recording solution at room temperature (20–23 °C). Oocytes were impaled with two microelectrodes and clamped at a holding voltage of −80 mV. Outward K^+ currents were evoked with 300-ms pulse steps of 20 mV from −80 to 60 mV in 5-s intervals using Clampex 10.5 software (Molecular Devices). To evaluate inhibition, at least two batches of oocytes, with 10 oocytes in each group, were recorded 2 days after cRNA injection. Oocytes that have robust outward K^+ currents at positive voltages and a leak current less than 0.1 μA at −80 mV are best for study. Data for control groups (KcsA-Shaker alone) and T-toxin groups were analyzed off-line using pCLAMP 10.5 and Excel. The mean value of current amplitudes at 0 mV for KcsA-Shaker channels without (control, $I_{control}$), or with 0.5 ng T-HmK cRNA co-injection (T_{toxin}) were used to determine the extent of inhibition ($F_{un} = I_{toxin}/I_{control}$), showing co-injection of 0.5 ng T-HmK cRNA inhibited 94% of the KcsA-Shaker current (Fig. 1B).

3. Reversing T-HmK inhibition of KcsA-Shaker to assess equilibrium affinity in single oocytes is described in Section 3 on kinetics of blockade. T-toxins were designed with a c-Myc epitope in the linker between the HmK sequence and GPI anchor (Fig. 1A) allowing reversal of inhibition on application of anti-c-Myc antibody (9E10).
4. Quantification of T-HmK surface level by ELISA. 2 days after injection, the surface expression of T-HmK and T-RFP were compared using ELISA. Individual oocytes were placed in Flat Bottom Nunc 96-Well microplates (one oocyte per well) and bathed for 2 h in recording solution with 3% BSA (200 μL/well) at 16 °C. After three washes with recording solutions, oocytes were incubated with 1 μg/mL anti-Myc-HRP (Invitrogen) for 1 h in recording solution with 3% BSA at 16 °C. Oocytes were washed five times using Recording solution with 0.1% Tween 20 and then twice more using Recording solution without Tween 20. Oocytes were then transferred to Conical Bottom Nunc 96-Well microplates with 50 μL 1-Step Ultra TMB-ELISA solution in each well and incubated for 15 min at room temperature. The reaction was stopped by adding 50 μL of 2 M H_2SO_4. Surface ELISA signals were quantitated at 450 nm using the Epoch microplate spectrophotometer. Oocytes without injected cRNA served as the negative control. For each construct, 12 oocytes from two batches were used for ELISA, and the results were analyzed off-line using Excel to obtain the mean value. ELISA signals for T-HmK and T-RFP were related such that with equimolar cRNA injection, the optical signal with T-RFP was ~77% of that for T-HmK (Fig. 2A) (Zhao et al., 2020).
5. Counting of individual T-RFP molecules on oocytes surface using smTIRF. 2 days after 0.5 ng T-RFP cRNA injection, *Xenopus* oocytes were devitellinized manually, and placed on glass bottom dishes (Chemglass Life Science) with recording solution bath. Oocyte surfaces were studied with a high numerical aperture apochromat objective (150 ×) mounted on an automated fluorescence microscope (Olympus) controlled by Metamorph software (Molecular Devices). The critical angle for TIRF was reached using Metamorph to illuminate ~100 nm of oocyte surface (Fig. 2B). RFP fluorophores were excited with the 561 nm laser line and recorded by a back-illuminated EM-CCD. Data was recorded as movies of 300 frames acquired at 1 Hz with continual excitation as routine (Plant, Xiong, Dai, & Goldstein, 2014; Zhao et al., 2018). For each oocyte, four regions (two in the animal hemisphere

and two in the vegetal hemisphere) were recorded to assure the distribution of T-RFP was uniform. The surface particle number of T-RFP in the first frame of movies from the four separate regions ($10 \times 10\,\mu m$ field) was manually counted using ImageJ software. The average number of single particles per $100\,\mu m^2$ was ~16 when oocytes were injected with 0.5 ng T-RFP cRNA (Fig. 2B).

6. Calculating the T-HmK concentration ([Tx]) on the oocyte surface. The average capacitance of oocytes is ~200 nF (C) (Schmitt & Koepsell, 2002; Zhao et al., 2020) and the specific membrane capacitance of stage VI oocytes is $\sim 4\,\mu F/cm^2$ (c) (Baker, Dunn, Holt, & Lajtha, 2006). The total oocyte surface area (S) is $\sim 5 \times 10^6\,\mu m^2$ given by $S = C/c$. The average number of single T-RFP particles (n_{RFP}) in a $100\,\mu m^2$ membrane surface area (s) is obtained by smTIRF counting. For example, when 0.5 ng T-RFP cRNA injection yields a mean $n_{RFP} \sim 16$, the average number of T-RFP peptides on the whole oocyte surface (N_{RFP}) is estimated to be $\sim 8 \times 10^5$ given by $N_{RFP} = (S/s)n_{RFP}$. ELISA shows that the expression level of T-RFP is 77% of that for T-HmK. Thus, the estimated N for T-HmK is $\sim 1 \times 10^6$ given a determination of $N_{RFP} = 0.77\,N$. This can be converted to moles ($mol_{HmK} = \sim 2.2 \times 10^{-18}$ mol) per $mol_{HmK} = N/NA$, where NA is Avogadro's number. Finally, the reaction volume (V) available to T-toxin can be estimated as the area between two spheres (Fig. 1C). The smaller sphere has a radius equal to the average radius of oocyte ($r = \sim 0.6$ mm). For T-HmK, the bigger sphere radius (R) is estimated to be r plus the full extent of the 46-residue peptide linker (number of residues × 3 Å for each peptide bond, ~138 Å), the length of sugar chain of the GPI anchor (~60 Å), and the diameter of HmK toxin (28 Å), that is, $46 \times 3 + 60 + 28 = 226$ Å (Fig. 1B). The reaction volume given by $V = (4/3)(\pi R^3 - \pi r^3)$ is thus $\sim 1 \times 10^{-10}$ L. The [Tx] of T-HmK can calculated from the ratio of molar amount of T-HmK (mol_{HmK}) and the reaction volume (V). For a 0.5 ng T-HmK cRNA injection, the estimated effective T-HmK concentration given by $[Tx] = mol_{HmK}/V$ is ~17 nM.

7. Calculating the K_i of T-HmK. Given a bimolecular interaction between a pore blocking toxin and a K^+ channel (MacKinnon & Miller, 1988), the apparent K_i of toxins can be calculated using Eq. (1) (Goldstein & Miller, 1993):

$$F_{un} = (1 + [Tx]/K_i)^{-1} \quad (1)$$

As co-injection of 0.5 ng T-HmK cRNA inhibited 94% of the KcsA-Shaker current ($F_{un} = 0.06$) in TEVC and [Tx] = 17 nM based on ELISA and smTIRF, as described above, the K_i of T-HmK is 1 nM per Eq. (1). When T-HmK cRNA was injected in amounts from 0.01 to 1 ng, inhibition increased from 2% to 98% (Zhao et al., 2020). The [Tx] of T-HmK with various injected cRNA levels was determined using ELISA and smTIRF and a fit of the concentration-response relationship also yielded a K_i of 1 nM with a Hill coefficient of 1 (Fig. 2C).

2.4 Alternatives

1. Consideration of T-toxin design. The characteristics of the toxin and channel will influence the effectiveness of various linker lengths for a new T-toxin. Blockade by T-toxins is comparable to free peptide analogs and tethering allows study even of low affinity toxins because they can achieve high local concentration given accommodation for steric constraints (Zhao et al., 2020). Thus, design of linker region is important to achieve optimal T-toxin efficacy. When we assessed T-HmK toxins with linkers varying from 6 residues to 66 residues (using Gly-Asn repeats) we found that a linker of 26 residues was required to allow T-HmK to reach its binding site in KcsA-Shaker pore (Zhao et al., 2020). Conversely, the tethered form of the neuropeptide pigment dispersing factor (t-PDF) had greatest activity when a short linker was used (Choi et al., 2009). The linker length determines the reaction volume and effective concentration of T-toxins on oocyte membrane surface (Zhao et al., 2020). As noted, above toxins that require a free C-terminus, non-canonical residues or post-translational modifications to interact with the target may not be amenable to T-toxin studies.
2. T-toxin and receptor cRNA injection ratio. After determining the level of cRNA injection to measure KcsA-Shaker current reproducibly, T-HmK cRNA was injected from 0.01 to 1 ng and inhibition increased from 2% to 98% allowing construction of a dose response curve and identification of an optimal ratio for scanning mutagenesis studies described in Section 4 (Zhao et al., 2020).
3. T-toxins in mammalian cells. T-toxins have been used successfully in native and cultured mammalian cells (Ibanez-Tallon & Nitabach, 2012). The challenge to be expected if the goal is to quantify block parameters, rather than suppress all activity, is that while delivery of

defined ratios of T-toxin and receptor may be achieved by transient transfection of plasmid mixtures, the level of expression from cell-to-cell will vary producing a spread in the concentration of the toxin in the outer membrane leaflet that might be mitigated in part by use of fluorescent tags to favor selection of comparable cells.

4. Releasing channels from steady-state T-toxin inhibition. We used anti-Myc to release KcsA-Shaker currents from T-HmK inhibition (Zhao et al., 2020). Anti-Myc binds to the c-Myc epitope encoded in the flexible T-HmK linker region (Fig. 1B), presumably reducing linker flexibility or creating a T-toxin-antibody complex that is too large to re-enter to the pore vestibule. Using the method, KcsA-Shaker currents can be restored to the levels measured when no T-HmK is expressed in the cells (Zhao et al., 2020). As an alternative, phosphatidylinositol-specific phospholipase C (PI-PLC) cleaves GPI anchors and releases tethered proteins from the cell surface. Thus, it was shown that PI-PLC restores the voltage-gated Na^+ current from T-MrVIa blockade (Sturzebecher et al., 2010). Optical control of T-toxin binding and release has also been achieved although the overlapping kinetics of the conformational changes of the photoswitch and T-toxin blockade make biophysical characterization challenging (Schmidt, Tillberg, Chen, & Boyden, 2014).
5. Estimating T-HmK surface concentration. We quantify T-RFP and T-HmK expression by comparative ELISA and counting T-RFP surface density using smTIRF. Two other methods allow direct assessment. First, a fluorescent protein like RFP can be incorporated into T-toxin between the sequence of signal peptide and toxin if a free N-terminus is not required for target binding (Auer et al., 2010) to allow direct visualization of extracellular GPI anchored T-toxin using smTIRF. Second, the GPI anchor of T-toxins can be replaced with a transmembrane domain from the platelet-derived growth factor receptor (PDGF) allowing encoding of a fluorescent protein to the intracellular portion of the expression construct (Auer et al., 2010).

3. Determining the kinetics of T-HmK inhibition (Fig. 3)

Toxin block that proceeds by a bimolecular reaction can be described as the ratio of the first-order dissociation rate constant (k_{off}) and the second-order association rate constant (k_{on}) according to Eq. (2), and this

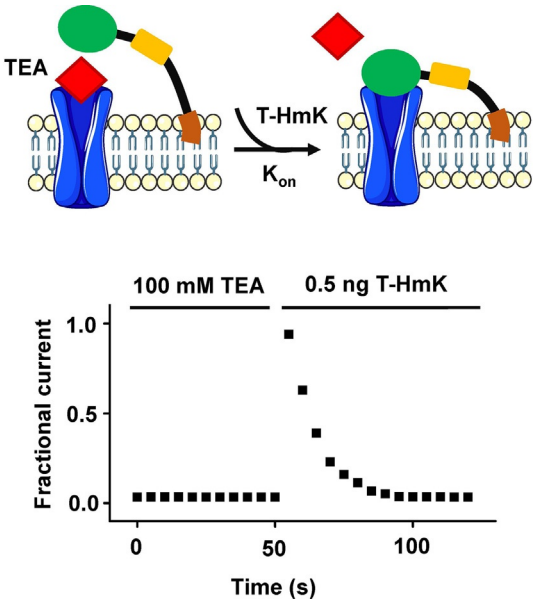

Fig. 3 Association kinetics of T-HmK can be revealed after rapid TEA unblock. TEA blocks KcsA-Shaker (100 mM) from the outside and prevents T-HmK binding. Unblock by TEA is rapid (less than 1 5-s interpulse interval) so full unblocked current is recorded on TEA washout before there is significant re-association and blockade by T-HmK. T-HmK relaxes to equilibrium blockade ($\tau \sim 8$ s with 0.5 ng T-HmK cRNA).

is related to F_{un} (Eq. 1) according to Eq. (3) (Goldstein & Miller, 1993; Kuriyan, Konforti, & Wemmer, 2013):

$$K_i = k_{off}/k_{on} \tag{2}$$

$$F_{un} = k_{off}/(k_{on}[Tx] + K_{off}) \tag{3}$$

Furthermore, k_{on} and k_{off} are related to the association constant (τ_{on}) and dissociation constant (τ_{off}) derived from single exponential fits of the time courses for block and unblock by Eqs. (4) and (5) (Goldstein & Miller, 1993; Kuriyan et al., 2013).

$$\tau_{on} = (k_{on}[Tx] + k_{off})^{-1} \tag{4}$$

$$\tau_{off} = (k_{off})^{-1} \tag{5}$$

Applying free peptides in solution to oocytes expressing ion channels allows direct measurement of the kinetics of current block and unblock through study of toxin wash-in and wash-off (Goldstein et al., 1994; Zhao et al., 2015). In contrast, when ion channels are expressed with T-toxins, they

are blocked at baseline because the toxin is fixed to the membrane by its tether. To study unblocked KcsA-Shaker channels, we employed TEA, an organic cation blocker of K^+ channel pores (Lu et al., 2001) to displace the T-HmK from the pores, and since its unblock kinetics are so rapid, we can study tethered-toxin re-binding to measure the association rate (Fig. 3) (Zhao et al., 2020). The dissociation rate is calculated from the measured association rate and equilibrium affinity as noted next.

3.1 Measuring association rate and calculating disassociation rate of T-HmK inhibition

3.1.1 Materials

Tetraethylammonium (TEA) solution contains in mM: 4 KCl, 100 TEA, 0.3 $CaCl_2$, 1 $MgCl_2$, 10 HEPES, pH 7.5.

Otherwise, as described in Section 2.1.

3.1.2 Equipment

As described in Section 2.2.

3.1.3 Protocol

1. Measuring the association rate of T-HmK via rapid TEA unblock. TEA block of KcsA-Shaker has a K_i of ~0.8 mM (Lu et al., 2001). TEA competes with T-HmK for binding in the outer pore because their sites overlap (Zhao et al., 2020). Bathing the cells with 100 mM TEA blocks KcsA-Shaker channels fully despite low affinity TEA because the high concentration yields rapid occupancy of the pore (Fig. 3). When oocytes expressing T-HmK and KcsA-Shaker were incubated in TEA solution containing 100 mM TEA for 1 h, TEA replaces T-HmK in the pore because it moves in rapidly on T-HmK unbinding (Fig. 3).
2. Oocytes in TEA solution were transferred to the TEVC recording chamber. Then, K^+ currents were evoked from a holding voltage of −80 mV with repetitive 300-ms test pulses to 0 mV with a 5-s interpulse interval and recorded as described in Section 2.3. When the currents were stable, the bath perfusion was switched to Recording solution. The dissociation of TEA was adequate ($\tau_{off} \sim 1.3$ s) with this flow apparatus to be fully washed off the channels in less than one recording sweep at the 5-s interval, allowing the slow association of T-HmK to be observed as a gradual decrease in the current decrease.
3. When 0.5 ng T-HmK cRNA was injected, the association of T-HmK determined from single exponential fits was $\tau_{on} = 8$ s (Fig. 3). Since

$K_i = 1$ nM and [Tx] = 17 nM, as described in Section 2.3, according to Eqs. (3) and (5), the k_{on} of T-HmK was 6.6×10^6 Ms^{-1} and the k_{off} was calculated to be 7.3×10^{-3} s^{-1} by Eq. (2).

3.1.4 Alternatives

T-toxins can be widely used for targeting numerous ion channels, while TEA is only sensitive to a subtype of K^+ channels (Heginbotham & MacKinnon, 1992). Fortunately, other ion channels can also be inhibited by low affinity inhibitors (Hille, 2001; Trudeau & Zheng, 2016) to allow a similar approach to evaluate the kinetics of T-toxin binding.

4. Identifying important residues for T-HmK binding by scanning mutagenesis (Fig. 4)

Scanning the residues of toxins to identify those with a role in ion channel binding blockade has proven valuable to reveal mechanisms of toxin action, the structure of the receptor site, and the development of agents that have improved potency and selectivity (Goldstein et al., 1994; MacKinnon & Miller, 1988; Murray et al., 2015). T-toxins provide a rapid and effective screening tool compared to soluble peptides because synthesis, purification, folding and storage are replaced by introduction of point mutations into T-toxin plasmid. cRNAs are produced from the variant T-toxin cDNAs and studied to assess inhibition (F_{un}) as described in Section 2. The change in affinity change is calculated using Eq. (6):

$$K_{i\ variant}/K_{i\ WT} = (1 - F_{un\ variant})\ F_{un\ WT}/(1 - F_{un\ WT})\ F_{un\ variant} \quad (6)$$

4.1 Scanning mutagenesis with T-toxins

4.1.1 Materials

QuikChange Site-Directed Mutagenesis Kit (Agilent).

Otherwise, as described in Section 2.1.

4.1.2 Equipment

The same as described in Section 2.2.

4.1.3 Protocol

1. Mutations of T-HmK were introduced using QuikChange Site-Directed Mutagenesis Kit at all sites except those involved in disulfide

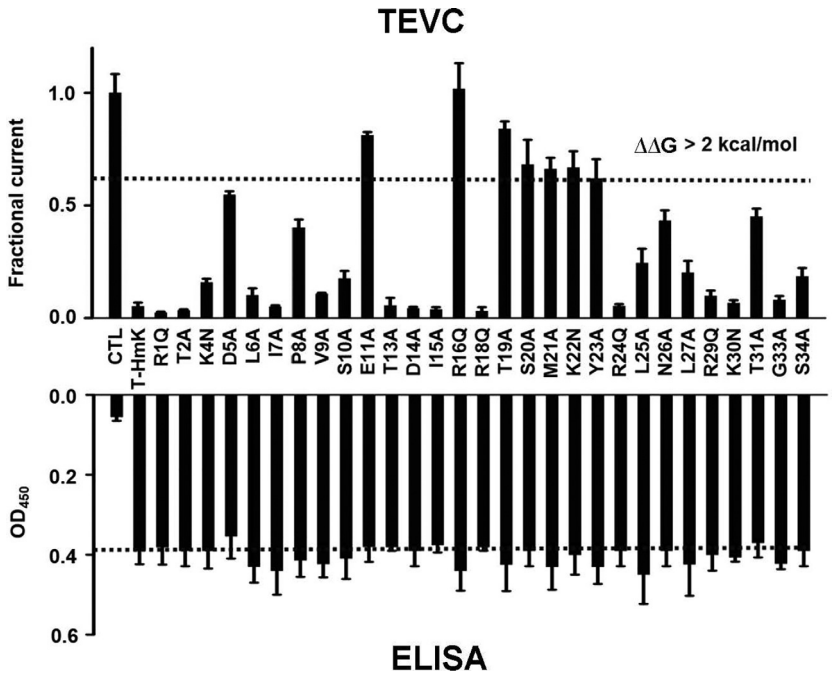

Fig. 4 T-HmK screening mutagenesis: measurement of KcsA-Shaker current and T-HmK surface expression level identifies residues critical to blockade. KcsA-Shaker current in oocytes and surface expression of WT T-HmK and T-HmK point variants were studied by TEVC and ELISA after co-inject 0.5 ng T-HmK cRNAs and 1 ng KcsA-Shaker cRNA. Top, KcsA-Shaker currents at 0 mV with T-HmK variants normalized to the unblocked condition (Control). $n = 16$–18 cells for each variant. Bottom, ELISA performed with T-HmK variants. Control was without the toxin. $n = 12$ cells for each condition.

bonds to produce 29 point mutants (Fig. 4). The plasmid sequences of all variants were confirmed by DNA sequencing.

2. cRNAs for the T-HmK variants were made as described in Section 2.1.
3. Oocytes were injected with 0.5 ng cRNA for each T-HmK variant (or WT T-HmK) with 1 ng KcsA-Shaker cRNA or, for the control group, only 1 ng KcsA-Shaker cRNA.
4. 2 days after injection, the surface expression of T-toxins variants was determined using ELISA as described in Section 2.3 to evaluate if any mutations have altered surface expression compared to WT T-HmK. Oocytes without injected cRNA served as the negative control, and oocytes injected with WT T-HmK cRNA served as the positive control. For each variant or control, 12 oocytes were studied by ELISA, and the results were analyzed off-line. None of the T-HmK mutants showed a significant change in surface expression (Fig. 4).

5. Inhibition by T-HmK variants of KcsA-Shaker channels was measured by TEVC as described in Section 2.3. For each variant, two batches with 10 oocytes each was recorded. The current-voltage relationships of recordings are analyzed and averaged off-line using Excel and the mean values of current amplitude at 0 mV were used to determine the extent of inhibition (F_{un}) as described in Section 2.3.
6. Inhibition by WT T-HmK of KcsA-Shaker currents was studied before and after recording T-toxin variants groups to confirm the extent of inhibition by WT T-toxin was unchanged during the study period and assuring that recording conditions were stable.
7. The change in affinity for a variant was calculated using Eq. (1). We identified seven T-HmK mutants that changed the free energy of toxin binding ($\Delta\Delta G$) more than 2 kcal/mol ($K_{i\ variant}/K_{i\ WT} > 26$-fold) per the equation: $\Delta\Delta G = RT \ln (K_{i\ variant}/K_{i\ WT})$, where R is the gas constant and T is temperature in Kelvin (Fig. 4). The seven residues map together on a continuous surface of the HmK 3D structure determined by NMR and were presumed to make close contact with KcsA pore (Zhao et al., 2020).

4.1.4 Alternatives

SAK-1 toxin peptides are relatively small (<37 residues) and the conserved backbone and three disulfide bonds allows ready, correct folding *in vitro* (Diochot & Lazdunski, 2009; Tudor et al., 1996). This may explain why we observed similar expression levels for T-HmK variants in oocytes (Fig. 4). This is not always the case. Point variants of T-ProTx-1, the other T-toxin that had been extensively scanned, showed notable variation in surface expression (Gui et al., 2014; Rupasinghe et al., 2020). This is not a surprise given that ProTx-1 has an inhibitor cystine knot (ICK) scaffold and both expression and folding of ICK toxins has been proven to present challenges *in vitro* (Swartz, 2007). This highlights the importance of confirming the surface concentration as described in Section 2.3.

5. Determining T-HmK blocking mechanism (Fig. 5)

The scorpion toxin CTX blocks K^+ channels by positioning Lys_{27} in the ion conduction pore to impede passage of K^+ ions (Banerjee, Lee, Campbell, & Mackinnon, 2013; Goldstein et al., 1994; Park & Miller, 1992). This was long accepted as the exclusive blockade mechanism for K^+ channel pore occluding toxins (Rauer, Pennington, Cahalan, & Chandy, 1999), until several recent reports (Moldenhauer, Diaz-Franulic,

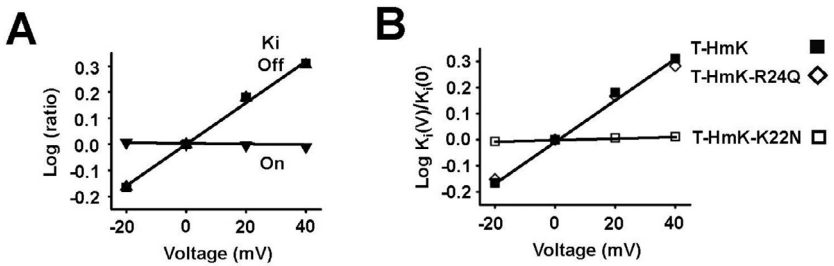

Fig. 5 Voltage-dependent block of KcsA-Shaker channels is mediated by T-HmK-Lys_{22}. KcsA-Shaker was expressed in oocytes, and inhibition by T-HmK and T-Hmk point variants were studied by TEVC after co-inject 0.5 ng cRNAs and 1 ng KcsA-Shaker cRNA. (A) Effect of voltage on T-HmK block kinetics; the on-rate is insensitive to voltage whereas the off-rate changes, consistent with a trans-ion knock-off effect. Each parameter was measured with test steps from −20 to 40 mV and normalized to the value at 0 mV; ▼, k_{on}; ▲, k_{off}; ■, K_i. K_i was determined from the fraction of unblocked current at equilibrium (F_{un}) according to Eq. (1). The association constant was determined by single exponential fits to the time course for T-HmK inhibition after TEA wash-off as in Fig. 3. The dissociation rate constant was determined from K_i and k_{on} according to Eq. (2). (B) Effect of voltage on block by T-HmK mutants; neutralizing Lys_{22} (K22N) but not Arg_{24} (R24Q) removes the voltage dependence of T-HmK blockade of KcsA-Shaker. K_i for each variant was determined from −20 to 40 mV based on the fraction of unblocked current at equilibrium (F_{un}) and plotted as a ratio to the value at 0 mV.

Poblete, & Naranjo, 2019; Sumino, Sumikama, Uchihashi, & Oiki, 2019; Zhao et al., 2015, 2020). CTX block is sensitive to voltage because the positively charged ε-amino group of its Lys_{27} enters the external portion of the pore and is repelled by the K^+ ions traversing pathway from the intracellular compartment, increasing the toxin off-rate (Goldstein & Miller, 1993; MacKinnon & Miller, 1988). We also observed this mechanism for HmK, but not two other SAK-1 toxins, Hui1 and ShK, which block K^+ channels via an Arg-dependent mechanism (Zhao et al., 2020). This alternate mode of pore occlusion was revealed by comparing the inhibition by WT T-toxins (where trans-ions enhanced toxin dissociation, a knock-off effect) and T-toxin variants where the charged interaction residues were neutralized and the voltage dependence of inhibition was eliminated.

5.1 Protocol for measuring the voltage-dependent inhibition of T-HmK variants

5.1.1 Materials

The same as described in Section 2.1.

5.1.2 Equipment

The same as described in Section 2.2.

5.1.3 Protocol

1. Positively-charged interaction residues in T-HmK (Lys_{22} and Arg_{24}) were neutralized by mutation (to Asn and Gln, respectively) as described in Section 4.1.3 (Fig. 4).
2. cRNAs for T-HmK variants were produced as described in Section 2.1.
3. Oocytes were injected with 0.5 ng cRNA for each T-HmK variant (or WT T-HmK) with 1 ng KcsA-Shaker cRNA or, for the control group, only 1 ng KcsA-Shaker cRNA.
4. Determining the voltage dependence of T-toxin K_{off}. The F_{un} and K_{on} of T-HmK at different voltages were measured as described in Sections 2.3 and 3.1.3 (−20, 0, 20 and 40 mV) and K_i and K_{off} calculated according to Eqs. (1) and (2). For the WT T-toxin the off-rate increases with depolarization as expected for trans-ion knock-off. Another way of describing the voltage dependence is effective valence (zδ) of WT T-HmK, ∼0.4 (Zhao et al., 2020) according to $\mathrm{Log}(K_{off\ pulse\ voltage}/K_{off\ 0\ mV}) = z\delta F(V_{pulse\ voltage})/RT$, where F is Faraday's constant, R is the gas constant and T is temperature in Kelvin (Goldstein & Miller, 1993).
5. Identifying the pore occluding residue by mutation. Because T-HmK blocks via the canonical Lys-mediated mechanism, neutralizing Lys_{22} removed the voltage dependence of off-rate whereas neutralizing Arg_{24} has no effect (Fig. 5). Neutralization of the pore occluding residue eliminated the voltage dependence of K_{off} to yield $z\delta \sim 0$.

6. Summary

T-toxins can facilitate the study of peptide toxins and their use has been successfully demonstrated with native and designer toxins in wild type and mutant form on a variety of ion channels and membrane receptors. Advantages include rapid study of many different peptides at low cost. The method allows study of peptides predicted by genomic screens, that are hard to isolate or synthesize, or have low affinity. The strategy allows determination of potency, mechanism of action and facilitates both screening of the role of individual resides and the functional effects of subsequent peptide engineering.

References

Auer, S., Sturzebecher, A. S., Juttner, R., Santos-Torres, J., Hanack, C., Frahm, S., et al. (2010). Silencing neurotransmission with membrane-tethered toxins. *Nature Methods*, 7, 229–236.

Baker, G., Dunn, S., Holt, A., & Lajtha, A. (2006). *Handbook of neurochemistry and molecular neurobiology: Practical neurochemistry methods*. New York, NY: Springer.

Banerjee, A., Lee, A., Campbell, E., & Mackinnon, R. (2013). Structure of a pore-blocking toxin in complex with a eukaryotic voltage-dependent K(+) channel. *eLife*, *2*, e00594.
Bosmans, F., Martin-Eauclaire, M. F., & Swartz, K. J. (2008). Deconstructing voltage sensor function and pharmacology in sodium channels. *Nature*, *456*, 202–208.
Castaneda, O., Sotolongo, V., Amor, A. M., Stocklin, R., Anderson, A. J., Harvey, A. L., et al. (1995). Characterization of a potassium channel toxin from the Caribbean Sea anemone Stichodactyla helianthus. *Toxicon*, *33*, 603–613.
Chandy, K. G., & Norton, R. S. (2017). Peptide blockers of Kv1.3 channels in T cells as therapeutics for autoimmune disease. *Current Opinion in Chemical Biology*, *38*, 97–107.
Choi, C., Fortin, J. P., McCarthy, E., Oksman, L., Kopin, A. S., & Nitabach, M. N. (2009). Cellular dissection of circadian peptide signals with genetically encoded membrane-tethered ligands. *Current Biology*, *19*, 1167–1175.
Cordeiro, S., Finol-Urdaneta, R. K., Kopfer, D., Markushina, A., Song, J., French, R. J., et al. (2019). Conotoxin kappaM-RIIIJ, a tool targeting asymmetric heteromeric Kv1 channels. *Proceedings of the National Academy of Sciences of the United States of America*, *116*, 1059–1064.
Cotton, J., Crest, M., Bouet, F., Alessandri, N., Gola, M., Forest, E., et al. (1997). A potassium-channel toxin from the sea anemone Bunodosoma granulifera, an inhibitor for Kv1 channels. Revision of the amino acid sequence, disulfide-bridge assignment, chemical synthesis, and biological activity. *European Journal of Biochemistry*, *244*, 192–202.
Diochot, S., & Lazdunski, M. (2009). Sea anemone toxins affecting potassium channels. *Progress in Molecular and Subcellular Biology*, *46*, 99–122.
Doyle, D. A., Morais Cabral, J., Pfuetzner, R. A., Kuo, A., Gulbis, J. M., Cohen, S. L., et al. (1998). The structure of the potassium channel: Molecular basis of K+ conduction and selectivity. *Science*, *280*, 69–77.
Gendeh, G. S., Young, L. C., de Medeiros, C. L., Jeyaseelan, K., Harvey, A. L., & Chung, M. C. (1997). A new potassium channel toxin from the sea anemone Heteractis magnifica: Isolation, cDNA cloning, and functional expression. *Biochemistry*, *36*, 11461–11471.
Goldstein, S. A., & Miller, C. (1993). Mechanism of charybdotoxin block of a voltage-gated K+ channel. *Biophysical Journal*, *65*, 1613–1619.
Goldstein, S. A., Pheasant, D. J., & Miller, C. (1994). The charybdotoxin receptor of a Shaker K+ channel: Peptide and channel residues mediating molecular recognition. *Neuron*, *12*, 1377–1388.
Gui, J., Liu, B., Cao, G., Lipchik, A. M., Perez, M., Dekan, Z., et al. (2014). A tarantula-venom peptide antagonizes the TRPA1 nociceptor ion channel by binding to the S1-S4 gating domain. *Current Biology*, *24*, 473–483.
Heginbotham, L., & MacKinnon, R. (1992). The aromatic binding site for tetraethylammonium ion on potassium channels. *Neuron*, *8*, 483–491.
Hille, B. (2001). *Ion channels of excitable membranes*. Sunderland, MA: Sinauer.
Ibanez-Tallon, I., Miwa, J. M., Wang, H. L., Adams, N. C., Crabtree, G. W., Sine, S. M., et al. (2002). Novel modulation of neuronal nicotinic acetylcholine receptors by association with the endogenous prototoxin lynx1. *Neuron*, *33*, 893–903.
Ibanez-Tallon, I., & Nitabach, M. N. (2012). Tethering toxins and peptide ligands for modulation of neuronal function. *Current Opinion in Neurobiology*, *22*, 72–78.
Ibanez-Tallon, I., Wen, H., Miwa, J. M., Xing, J., Tekinay, A. B., Ono, F., et al. (2004). Tethering naturally occurring peptide toxins for cell-autonomous modulation of ion channels and receptors in vivo. *Neuron*, *43*, 305–311.
Jiang, D., Tonggu, L., Gamal El-Din, T. M., Banh, R., Pomes, R., Zheng, N., et al. (2021). Structural basis for voltage-sensor trapping of the cardiac sodium channel by a deathstalker scorpion toxin. *Nature Communications*, *12*, 128.

Kalia, J., Milescu, M., Salvatierra, J., Wagner, J., Klint, J. K., King, G. F., et al. (2015). From foe to friend: Using animal toxins to investigate ion channel function. *Journal of Molecular Biology*, *427*, 158–175.

Kuriyan, J., Konforti, B., & Wemmer, D. (2013). *The molecules of life: Physical and chemical principles*. Garland Science.

Lanigan, M. D., Kalman, K., Lefievre, Y., Pennington, M. W., Chandy, K. G., & Norton, R. S. (2002). Mutating a critical lysine in ShK toxin alters its binding configuration in the pore-vestibule region of the voltage-gated potassium channel, Kv1.3. *Biochemistry*, *41*, 11963–11971.

Lu, Z., Klem, A. M., & Ramu, Y. (2001). Ion conduction pore is conserved among potassium channels. *Nature*, *413*, 809–813.

MacKinnon, R., & Miller, C. (1988). Mechanism of charybdotoxin block of the high-conductance, Ca2+-activated K+ channel. *The Journal of General Physiology*, *91*, 335–349.

MacKinnon, R., & Miller, C. (1989). Mutant potassium channels with altered binding of charybdotoxin, a pore-blocking peptide inhibitor. *Science*, *245*, 1382–1385.

Miwa, J. M., Ibanez-Tallon, I., Crabtree, G. W., Sanchez, R., Sali, A., Role, L. W., et al. (1999). lynx1, an endogenous toxin-like modulator of nicotinic acetylcholine receptors in the mammalian CNS. *Neuron*, *23*, 105–114.

Moldenhauer, H., Diaz-Franulic, I., Poblete, H., & Naranjo, D. (2019). Trans-toxin ion-sensitivity of charybdotoxin-blocked potassium-channels reveals unbinding transitional states. *eLife*, *8*, e46170. https://doi.org/10.7554/eLife.46170.

Murray, J. K., Qian, Y. X., Liu, B., Elliott, R., Aral, J., Park, C., et al. (2015). Pharmaceutical optimization of peptide toxins for ion channel targets: Potent, selective, and long-lived antagonists of Kv1.3. *Journal of Medicinal Chemistry*, *58*, 6784–6802.

Park, C. S., & Miller, C. (1992). Interaction of charybdotoxin with permeant ions inside the pore of a K+ channel. *Neuron*, *9*, 307–313.

Plant, L. D., Xiong, D., Dai, H., & Goldstein, S. A. (2014). Individual IKs channels at the surface of mammalian cells contain two KCNE1 accessory subunits. *Proceedings of the National Academy of Sciences of the United States of America*, *111*, E1438–E1446.

Rauer, H., Pennington, M., Cahalan, M., & Chandy, K. G. (1999). Structural conservation of the pores of calcium-activated and voltage-gated potassium channels determined by a sea anemone toxin. *The Journal of Biological Chemistry*, *274*, 21885–21892.

Rupasinghe, D. B., Herzig, V., Vetter, I., Dekan, Z., Gilchrist, J., Bosmans, F., et al. (2020). Mutational analysis of ProTx-I and the novel venom peptide Pe1b provide insight into residues responsible for selective inhibition of the analgesic drug target NaV1.7. *Biochemical Pharmacology*, *181*, 114080.

Schmidt, D., Tillberg, P. W., Chen, F., & Boyden, E. S. (2014). A fully genetically encoded protein architecture for optical control of peptide ligand concentration. *Nature Communications*, *5*, 3019.

Schmitt, B. M., & Koepsell, H. (2002). An improved method for real-time monitoring of membrane capacitance in Xenopus laevis oocytes. *Biophysical Journal*, *82*, 1345–1357.

Stuhmer, W. (1998). Electrophysiologic recordings from Xenopus oocytes. *Methods in Enzymology*, *293*, 280–300.

Sturzebecher, A. S., Hu, J., Smith, E. S., Frahm, S., Santos-Torres, J., Kampfrath, B., et al. (2010). An in vivo tethered toxin approach for the cell-autonomous inactivation of voltage-gated sodium channel currents in nociceptors. *The Journal of Physiology*, *588*, 1695–1707.

Sumino, A., Sumikama, T., Uchihashi, T., & Oiki, S. (2019). High-speed AFM reveals accelerated binding of agitoxin-2 to a K(+) channel by induced fit. *Science Advances*, *5*, eaax0495.

Swartz, K. J. (2007). Tarantula toxins interacting with voltage sensors in potassium channels. *Toxicon*, *49*, 213–230.

Takacs, Z., Toups, M., Kollewe, A., Johnson, E., Cuello, L. G., Driessens, G., et al. (2009). A designer ligand specific for Kv1.3 channels from a scorpion neurotoxin-based library. *Proceedings of the National Academy of Sciences of the United States of America*, *106*, 22211–22216.

Trudeau, M. C., & Zheng, J. (2016). *Handbook of ion channels*. CRC Press.

Tudor, J. E., Pallaghy, P. K., Pennington, M. W., & Norton, R. S. (1996). Solution structure of ShK toxin, a novel potassium channel inhibitor from a sea anemone. *Nature Structural Biology*, *3*, 317–320.

Wulff, H., Christophersen, P., Colussi, P., Chandy, K. G., & Yarov-Yarovoy, V. (2019). Antibodies and venom peptides: New modalities for ion channels. *Nature Reviews. Drug Discovery*, *18*, 339–357.

Zhao, R., Dai, H., Mendelman, N., Chill, J. H., & Goldstein, S. A. N. (2020). Tethered peptide neurotoxins display two blocking mechanisms in the K(+) channel pore as do their untethered analogs. *Science Advances*, *6*, eaaz3439.

Zhao, R., Dai, H., Mendelman, N., Cuello, L. G., Chill, J. H., & Goldstein, S. A. (2015). Designer and natural peptide toxin blockers of the KcsA potassium channel identified by phage display. *Proceedings of the National Academy of Sciences of the United States of America*, *112*, E7013–E7021.

Zhao, R., Kennedy, K., De Blas, G. A., Orta, G., Pavarotti, M. A., Arias, R. J., et al. (2018). Role of human Hv1 channels in sperm capacitation and white blood cell respiratory burst established by a designed peptide inhibitor. *Proceedings of the National Academy of Sciences of the United States of America*, *115*, E11847–E11856.